Archives of Biochemistry and Biophysics 746 (2023) 109741

Contents lists available at ScienceDirect

Archives of Biochemistry and Biophysics

journal homepage: www.elsevier.com/locate/yabbi

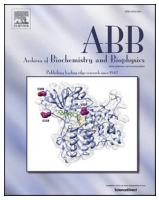

Effect of lipid oxidation on the channel properties of Cx26 hemichannels: A molecular dynamics study

Maria C. Oliveira [a,*], Rodrigo M. Cordeiro [b], Annemie Bogaerts [a]

[a] Plasma Lab for Applications in Sustainability and Medicine-Antwerp (PLASMANT), Department of Chemistry, University of Antwerp, Universiteitsplein 1, B-2610, Antwerp, Belgium
[b] Centro de Ciências Naturais e Humanas, Universidade Federal do ABC, Avenida dos Estados 5001, CEP 09210-580, Santo André, SP, Brazil

ARTICLE INFO

Keywords:
Gap junctions
Lipid oxidation
Molecular dynamics
Oxidative stress

ABSTRACT

Intercellular communication plays a crucial role in cancer, as well as other diseases, such as inflammation, tissue degeneration, and neurological disorders. One of the proteins responsible for this, are connexins (Cxs), which come together to form a hemichannel. When two hemichannels of opposite cells interact with each other, they form a gap junction (GJ) channel, connecting the intracellular space of these cells. They allow the passage of ions, reactive oxygen and nitrogen species (RONS), and signaling molecules from the interior of one cell to another cell, thus playing an essential role in cell growth, differentiation, and homeostasis. The importance of GJs for disease induction and therapy development is becoming more appreciated, especially in the context of oncology. Studies have shown that one of the mechanisms to control the formation and disruption of GJs is mediated by lipid oxidation pathways, but the underlying mechanisms are not well understood. In this study, we performed atomistic molecular dynamics simulations to evaluate how lipid oxidation influences the channel properties of Cx26 hemichannels, such as channel gating and permeability. Our results demonstrate that the Cx26 hemichannel is more compact in the presence of oxidized lipids, decreasing its pore diameter at the extracellular side and increasing it at the amino terminus domains, respectively. The permeability of the Cx26 hemichannel for water and RONS molecules is higher in the presence of oxidized lipids. The latter may facilitate the intracellular accumulation of RONS, possibly increasing oxidative stress in cells. A better understanding of this process will help to enhance the efficacy of oxidative stress-based cancer treatments.

1. Introduction

Cell-cell interactions play a pivotal role in physiological processes, such as cell development, tissue and organ homeostasis, neurotransmission, and immune response [1]. Failure or improper interactions result in a large variety of pathologies, such as skin and hair disorders, cardiomyopathies, sensory defects, psychiatric disorders, and cancers [2]. In vertebrates, cell-cell interactions can be classified into four functional classes: (i) adherens junctions, (ii) desmosomes; (iii) communicating junctions (or gap junctions (GJs)); and (iv) occluding junctions (or tight junctions) [2]. For this work, we will focus on GJs cell-cell interactions, which chemically and electrically couple neighbouring cells.

GJs consist of small gaps when two hemichannels (or connexons) of opposite cells interact with each other (Fig. 1A), allowing an intracellular communication between these cells. An assembly of six transmembrane proteins called connexins (Cxs) results in the formation of a hemichannel [3] (Fig. 1B). The human connexin (Cx) protein family contains 21 members, named according to their relative molecular mass, which can range from 23 to 62 kDa [4]. Each Cx is composed by four transmembrane (TM) domains in the α-helical conformation (TM1 to TM4). These domains are connected by two extracellular loops (EL-1 and EL-2) and one cytoplasmic loop (CL), containing an amino (NT) and carboxyl terminus (CT) in the cytoplasm [5] (Fig. 1C).

GJs are present in almost all human cells [6], and play an important role in the maintenance of physiological functions, such as cell growth, differentiation, homeostasis [7], angiogenesis [8], neural migration [9], and stem cell development [10]. They allow the transfer of various species directly from the interior of one cell to a neighbouring cell, including autocrine and paracrine signals (e.g. nicotinamide adenine dinucleotide (NAD^+) and adenosine triphosphate (ATP)), glutamate, glucose, and ions (e.g. Ca^{2+}, K^+, and Na^+), but also reactive oxygen and

* Corresponding author.
E-mail address: mariacecilia.oliveira@uantwerpen.be (M.C. Oliveira).

https://doi.org/10.1016/j.abb.2023.109741
Received 23 May 2023; Received in revised form 10 July 2023; Accepted 5 September 2023
Available online 7 September 2023
0003-9861/

nitrogen species (RONS) [4]. The permeability of GJs is regulated by changes in the membrane potential [11], phosphorylation [12], the presence of unsaturated fatty acids [13], changes in redox potential [14], pH [15], and alterations in extracellular Ca^{2+} [16] and Mg^{2+} [17] concentration. For instance, post-translational modifications, such as phosphorylation, oxidation, carbonylation, and C-terminal cleavage, have been shown to inhibit the GJ and hemichannel permeability [18]. Protein-protein interactions mediated by Cxs have also been able to modulate gap junction (GJ) channel function and regulation [19]. For instance, several reviews have summarized that interactions of Cxs with multiple proteins around it, which take place during Cx trafficking from the endoplasmic reticulum to the plasma membrane, are essential for GJ formation, membrane stabilization, and degradation [20–22]. Thus, knowledge of how biological molecules pass through GJ channels is extremely important.

The importance of GJs for disease induction and therapy development is becoming more appreciated, especially in the context of oncology. *In vitro* studies on solid tumor cells revealed that a lack of cell communication through GJs in certain tumor types results in abnormal cell growth [23]. Interestingly, restoration of GJs in tumor cell lines reduces tumor growth and proliferation [24]. This tendency was corroborated tracking Cx levels in cancer cells: a high Cx expression leads to better cancer prognosis, while a low Cx expression leads to a worse cancer prognosis [25]. For instance, a low expression of Cx46 proteins was found during differentiation of glioblastoma cancer stem cells, enhancing the cell-cell communication between cancer cells and consequently their self-renewal and tumor growth [26]. Once these outcomes may occur through both GJ-dependent pathways (based on Cx isoform, cancer type and stage) [27] and GJ-independent pathways (based on the CT domain of Cxs) [28–30], these results suggest that GJs and Cxs have anti-tumorigenic properties.

On the other hand, GJs and Cxs have also shown pro-tumorigenic properties. For example, Cx26 and Cx43 proteins were found to form GJs between endothelial cells or astrocytes (i.e., healthy cells) on one hand, and breast and melanoma cancer cells on the other hand, promoting metastasis and growth [31]. Altered levels of Cx26 and Cx43 proteins were also found in some subtypes of metastatic breast and lung cancer cells, when compared to the protein expression in primary tumor cells [32]. Additionally, mutations to the amino acid sequence of Cx26 proteins have also been associated with dysfunctions of hemichannels and GJs to cause many pathologies, such as skin diseases, peripheral and central neuropathic disorders, lens cataracts, and deafness [33,34]. To summarize, GJs and Cxs can have pro- and anti-tumorigenic properties, and its outcome depends on the GJ and Cx properties, tumor factors, and cancer stage [27,28].

Since GJs are able to transport a variety of biological molecules, e.g., RONS, from the interior of one cell to another cell, it is crucial to understand how this transport occurs and its effects on the cell function. For instance, RONS generated during oxidative stress-based cancer treatments (e.g., hydrogen peroxide (H_2O_2), hydroperoxyl radicals

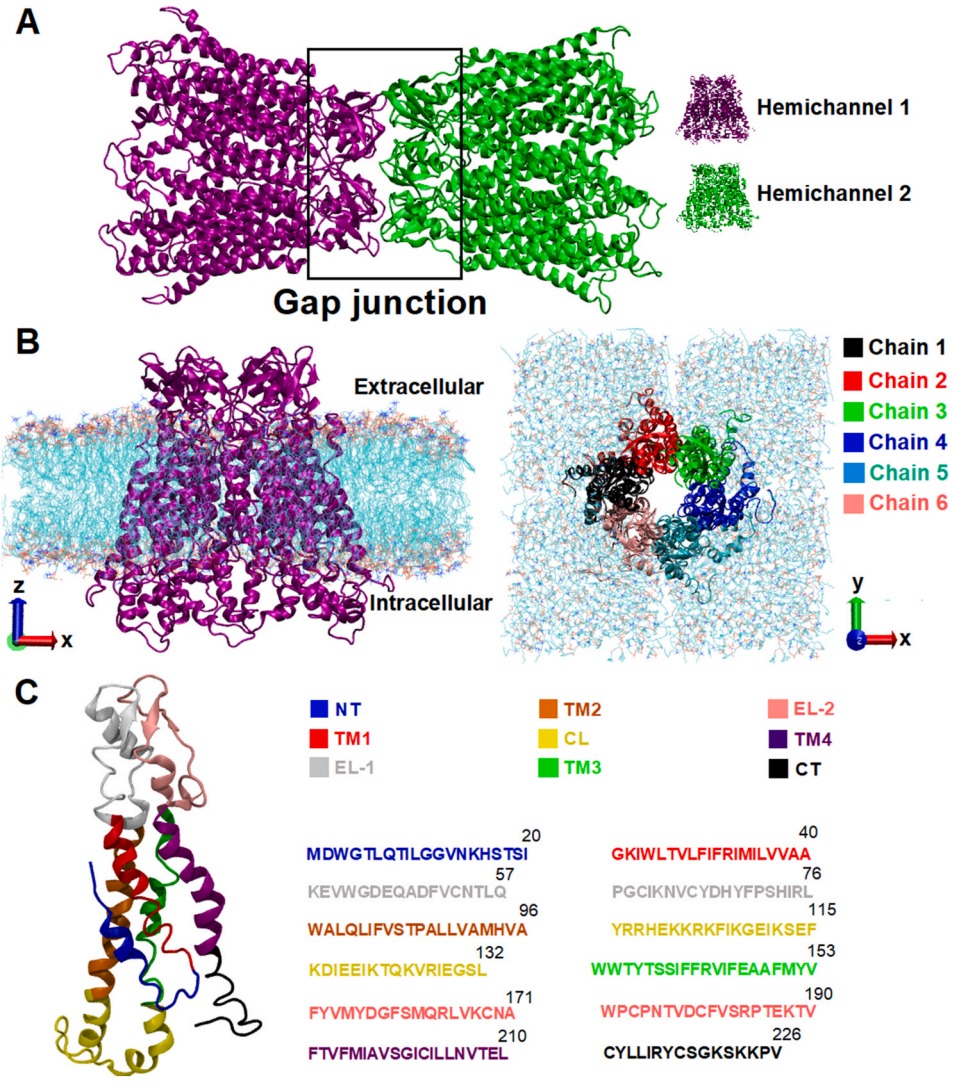

Fig. 1. Schematic representation of the Cx structure. (**A**) A gap junction channel of Cx26 proteins. Each hemichannel is represented as ribbons by a different colour (i.e., purple or green). The lipid bilayers (i.e., membranes) were removed for the sake of clarity. (**B**) Side view (left) and top view (right) of a Cx26 hemichannel (consisting of six Cx chains) embedded into a POPC (1-palmitoyl-2-oleoyl-*sn*-glycero-3-phosphocholine) lipid bilayer. The lipid bilayer is represented as lines of different colours. In the top view, each colour chain represents a single Cx26 protein. All chains (chain 1 to chain 6) are identical, and its structure can be seen in (**C**). It should be noted that there is an open and closed conformation of hemichannels, and the top view represents an open conformation. (**C**) Cx26 protein structure and its domains: transmembrane domains (TM1 (red), TM2 (orange), TM3 (green), and TM4 (purple)), extracellular loops (EL-1 (grey) and EL-2 (pink)), cytoplasmic loop (CL (yellow)), amino terminus (NT (blue)), and carboxyl terminus (CT (black)). The amino acid sequence of each domain is shown in different colours. The number for each sequence represents the position number of that amino acid residue in the domain.

($HO_2^{\bullet}$), hydroxyl radicals (HO•), singlet oxygen ($^1O_2$), and nitric oxide radicals ($^{\bullet}NO$)) are able to interact with the surface of cancer cells, and kill them by lipid and protein oxidation [35]. Consequently, the effects caused by RONS may also affect GJ function/activity. In fact, an increasing body of experimental evidence demonstrates that RONS can modulate GJs and hemichannels, either via direct effects on channel gating (pore opening/closing), or by affecting the intracellular trafficking of Cxs, impacting the number and stability of the GJ channel at the plasma membrane [36,37]. For instance, photodynamic therapy (PDT)-generated RONS were found to be able to improve Cx hemichannel activity and consequently, ATP release (paracrine signaling) from Cx hemichannels in syngeneic murine melanoma models *in vivo*, inducing bystander cell death and antitumor response via enhanced Ca^{2+} signaling [38]. These effects were greatly enhanced by combination treatment with S-nitrosoglutathione (GSNO), an endogenous $^{\bullet}NO$ radical donor that biases hemichannels towards the open state [38]. These results highlight Cx hemichannels as a potential target to increase cytotoxic bystander effects in cancer cells.

Likewise, lipid oxidation may also alter the properties of GJs and hemichannels. Studies have shown that GJ formation and disruption are modulated by lipid oxidation-mediated pathways [39,40], but the underlying mechanisms are not well understood and require further investigation. Lipid oxidation has also been found able to induce alteration in Cx expression and in phosphorylation, contributing to the pathogenesis of atherosclerosis [41]. Accordingly, lipid oxidation may also directly affect channel gating. For example, Retamal found that 4-hydroxy-2-nonenal (4-HNE), a reactive aldehyde derived from oxidized lipids, inhibits the Cx46 hemichannel activity in *Xenopus laevis* oocytes [42]. That inhibitory effect of 4-HNE on Cx46 hemichannels occurred through carbonylation of extracellular cysteines, inhibiting GJ formation and pointing out the importance of the disulfide bridges between extracellular cysteines in GJ formation [42]. Polyunsaturated fatty acids, such as linoleic acid and arachidonic acids, which can be easily oxidized, also inhibited the hemichannel activity *in vitro* [13]. Therefore, a plausible mechanism for hemichannel inhibition is through lipid oxidation.

The effect of lipid oxidation on the membrane properties has been largely studied both experimentally [43–45] and by simulations [46–48]. However, how it affects GJs and hemichannel properties still needs to be elucidated. In this study, we applied molecular dynamics (MD) simulations to study the effect of lipid oxidation on the channel properties of Cx26 hemichannels, more specifically the channel gating (opening/closing) and permeability. Several Cx proteins play a crucial role in cancer cell migration and metastasis, such as Cx26 [31,32], Cx32 [49], Cx43 [31,32,50], and Cx46 [51]. Although we are focused solely on Cx26 proteins in this work, we will consider exploring other Cx proteins in future studies.

2. Methods

2.1. Model systems and construction

The initial structure of the Cx26 hemichannel was taken from the Cx26-composed GJ channel (Cx26-GJ) at 3.5 Å resolution X-ray crystal structure, obtained by Maeda et al. [52]. The crystal structure of the Cx26-GJ was proposed to be an open channel, and can be obtained from the Protein Data Bank under the code 2ZW3. Due to the inherent flexibility of some domains in Cx26 hemichannels, several amino acid residues are missing in the crystal structure: residue 1 of the NT domains of the six Cx26 proteins, residues 110–124 of the CL domains, and residues 218–226 of the CT domains [52]. In principle, as our interest is to study the effect of lipid oxidation on the property of the Cx26 hemichannel pore, the missing of these amino acid residues may not affect our MD simulation results as a whole, since the channel pore is lined by amino acid residues in the N-terminal half of the EL-1 domains, the C-terminal half of the TM1 domains, the first half of the NT domains, and the C-terminal half of the TM2 domains [52] (see Fig. 1C). However, although the missing amino acid residues may not be pore-lining, Kwon et al. demonstrated later that the completion of the crystal structure affects the channel gating of the Cx26 hemichannel [53]. Thus, we simulated the completed Cx26 hemichannel structure taken from Albano and co-workers [54], based on the crystal structure of Maeda et al. [52].

The Cx26 hemichannel was embedded into either a 100% POPC (1-palmitoyl-2-oleoyl-*sn*-glycero-3-phosphocholine) lipid bilayer (POPC + Cx26) or a 100% oxidized POPC lipid bilayer into hydroperoxide –OOH group (POPCOOH + Cx26). POPC lipids are broadly used in biomimetic computational and experimental studies, since it is the major component of eukaryotic biological membranes [55]. Moreover, the experimental thickness of membranes composed of POPC lipids was measured as 38 Å [56], which is identical to the thickness of the TM domains in the crystal structure of the Cx26 GJ channel [52]. Likewise, lipid hydroperoxides are also widely studied, because they are one of the major products of oxidation of unsaturated fatty acids [57].

Each model system was composed of 500 lipid molecules (250 in each leaflet) solvated with a sufficient number of water molecules, to ensure proper hydration of the lipid bilayer and to prevent the interaction of the Cx26 hemichannel with itself. We packed the lipids around the Cx26 hemichannel using the InflateGRO program [58]. Sodium (Na^+) and chlorine (Cl^-) ions were randomly placed in the water at a concentration of 0.15 M, to neutralize the net charge of the Cx26 hemichannel and to mimic a physiological ionic strength. It should be pointed out that cholesterol molecules also play a very important role in membrane systems, since it regulates the membrane fluidity and permeability, as well as the formation of coexisting phases and domains in the membrane [59]. However, we have excluded cholesterol from our model systems in first instance, because it can also be oxidized, which would lead to a more complex membrane composition in terms of lipids and cholesterol oxidation products.

Figure S1 of the Supporting *Information* (SI) presents the initial structures of the simulated model systems. In Table S1 we summarize the characteristics of each model system described above. The structures of POPC and POPCOOH lipid molecules can be visualized in Figure S2. The –OOH groups are attached at the C9 carbon of oleoyl (*sn*-2) chains of POPCOOH lipid molecules, with *R* stereocenter (see Figure S2).

2.2. Molecular dynamics simulation parameters

All MD simulations were performed using GROMACS version 2020.2 [60], applying the united-atom GROMOS 54A7 force field [61]. We used well-validated models for the description of POPC [62] and POPCOOH lipids [63], and adopted interatomic interaction parameters for the amino acid residues from the standard GROMOS 54A7 force field library [61]. Water molecules were modeled with the simple point charge model [64]. Periodic boundary conditions were used in all cartesian directions. Newton's equations of motion were integrated using the leapfrog algorithm with a time step of 2 fs. A cut-off radius of 1.4 nm was used for non-bonded (Lennard-Jones and van der Waals) interactions. Coulomb interactions were treated using the reaction-field method [65]. The covalent bond lengths were constrained using the linear constraint solver (LINCS) algorithm [66].

We performed a steepest descent energy minimization, followed by a thermalization in the canonical ensemble (NVT) for 0.1 ns and an equilibration in the isothermal-isobaric ensemble (NPT) for 500 ns. The temperature was maintained at 310 K to maintain a disordered liquid state of the POPC lipids, by coupling the system to an external temperature bath using the Nose-Hoover thermostat [67,68]. The temperature coupling constant was 0.5 ps. The pressure was also maintained at around 1 bar by coupling the system to an external pressure bath using the Parrinello-Rahman barostat [69]. The pressure coupling was applied semi-isotropically, with a coupling constant of 2 ps and isothermal compressibility of 4.5×10^{-5} bar^{-1} [70].

2.3. Visualization and data analysis

Visualization of the simulated model systems and generation of the figures were carried out using the VMD software [71]. We used several built-in tools of GROMACS to perform analysis of the stability and dynamics of the Cx26 hemichannel: *gmx rms* for analysis of the root mean square deviation (RMSD), *gmx rmsf* for analysis of the root mean square fluctuation (RMSF), *gmx gyrate* for analysis of the radius of gyration (Rg), and *gmx rdf* for analysis of the radial distribution function (RDF). The bilayer thickness of the lipid bilayers (i.e., membranes) was defined as the average distance along the *z*-axis between the center of mass of the phosphorus atoms of both leaflets, using the *gmx traj* tool of GROMACS. The area per lipid (A_L) was calculated as:

$$A_L = \frac{L_x \times L_y}{n_L} \quad (1)$$

where L_x and L_y are the box length in the *x* and *y*-direction, respectively, and n_L is the number of lipids in each leaflet (i.e., 250).

For analysis of the permeability of the Cx26 hemichannel, we calculated the surface electrostatic potential with the adaptive Poisson-Boltzmann solver (APBS) program [72]. The pore profile was calculated using the Pore-Walker program [73]. Analysis of the density map was calculated using the *gmx densmap* and *gmx xpm2ps* tools of GROMACS. The angles within the Cx26 hemichannel was calculated using the *gmx gangle* tool of GROMACS. The polarity and charge of the Cx26 hemichannel was calculated using the MOLEonline program [74].

The distribution of water molecules along the Cx26 hemichannel pore was calculated using an in-house script, based on the number density of water molecules at different layers along pore-centered cylindrical cross sections. The cylinder had a radius of 7 Å and was oriented parallel to the *z*-axis. The free energy change (ΔG) associated with the transport of a water molecule from a distant point in solution to a specific position *z* inside the pore was calculated using the Boltzmann equation [75]:

$$\Delta G(z) = -k_B T \ln \frac{\rho(z)}{\rho_\infty} \quad (2)$$

where k_B is the Boltzmann constant, T is the temperature, $\rho(z)$ is the distance-dependent number density of water molecules and $\rho\infty$ is its bulk value.

3. Results and discussion

3.1. Stability and dynamics of Cx26 hemichannels

In order to assess the structural stability and dynamics of Cx26 hemichannels embedded in native (i.e., non-oxidized) and oxidized membranes, we calculated the RMSD of the protein alpha carbons (Cα), using as a reference the initial configuration structure of the hemichannel [54], and the Rg of the protein hemichannel in each model system. The RMSD is a measure of how much a structure deviates in position from a reference structure [76], and thus represents the stability of the whole system, whereas the Rg is a measure of the compactness of the system: the higher the Rg of the system is, the less compact is the system (loosest packing) [77]. Fig. 2 compares the RMSD and Rg of the Cx26 hemichannel embedded into POPC and POPCOOH membranes. As is apparent from Fig. 2, the systems are equilibrated after 300 ns of simulation time. Therefore, we performed all the analysis of the average quantities using the last 200 ns of the simulations, to eliminate any transient effects on the results presented.

The Cx26 hemichannel embedded into the POPCOOH membrane shows a slightly higher deviation from the reference structure than the Cx26 hemichannel embedded into the POPC membrane (Fig. 2A), i.e., Cx26 hemichannels embedded into oxidized membranes exhibit more conformational changes. Conformational changes of a protein are critical determinants for its biological function. For instance, conformational changes of particular proteins (e.g., unfolding, misfolding, and aggregation) have been correlated to many diseases, by toxic gain of a function, loss of a function, improper degradation, and improper localization [78,79]. On the other hand, conformational changes on pro-diseases proteins have also been used to hinder disease progression [80,81]. In Figure S3 we compare the structures of the initial configuration of the Cx26 hemichannel and of our equilibrated Cx26 hemichannels, showing that the intracellular side of the Cx26 hemichannel presents a higher deviation from the initial structure in the presence of oxidized lipids (see Figure S3). This result is in agreement with the higher conformational changes of the Cx26 hemichannel embedded into the POPCOOH membrane.

Interestingly, the Rg of the Cx26 hemichannel in the *xy* plane (i.e., along the *z*-axis of the membrane) is lower in the presence of oxidized lipids (Fig. 2B), suggesting that the Cx26 hemichannel is more compact in the oxidized membrane. Normally, more compact proteins require a higher folding time, and thus are more susceptible to undergo protein denaturation (unfolding). Indeed, Lobanov et al. performed statistical analysis of the Rg of several proteins, and demonstrated that α-proteins are less compact and fold more rapidly than β- and (α + β)-proteins [77].

To gather insight in the relative fluctuation of different regions within each Cx26 protein, we also evaluated the RMSF of each amino acid residue in the six different chains of the six Cx26 proteins that compose the hemichannel (Fig. 3). Similar fluctuation patterns are observed for the same Cx domains of the six chains. The highest fluctuations are observed within the NT (residues 1–20), EL-1 (residues

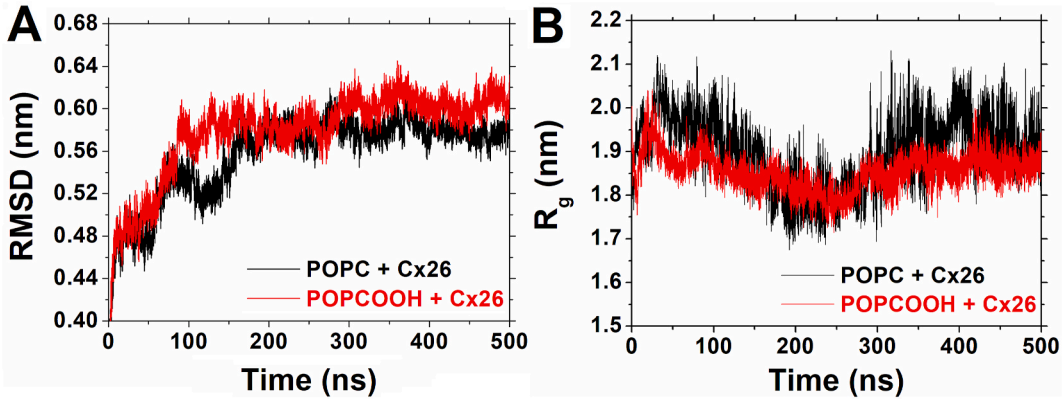

Fig. 2. Temporal evolution of the structural properties of the Cx26 hemichannel embedded into POPC and POPCOOH membranes: (**A**) average root mean square deviation (RMSD) and (**B**) average radius of gyration (Rg) in the *xy* plane of 10 slices along the *z*-axis. These data are an average of the 6 identical chains of the Cx26 hemichannel.

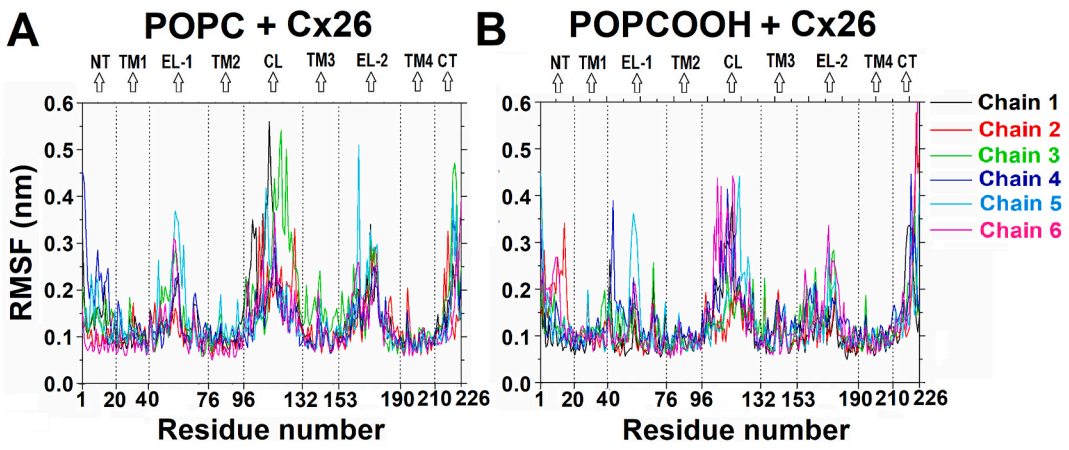

Fig. 3. Average root mean square fluctuation (RMSF) of each amino acid residue of the Cx26 hemichannel embedded into (**A**) the POPC membrane and (**B**) the POPCOOH membrane, calculated from the last 200 ns of simulation. Each colour chain represents the trajectory of a single Cx26 protein that composes the hemichannel.

41–76), CL (residues 97–132), EL-2 (residues 154–190), and CT (residues 211–226) domains (see Fig. 3). This is expected, since these domains are located outside the membrane, so they are more flexible because of their lack of structural constrains imposed by the membrane. Thus, the TM domains are the most stables regions, since they are embedded in the membrane and organized in α-helices, which restrict their movements. We can notice higher RMSF values when the Cx26 hemichannel is embedded into the POPC membrane than when embedded into the POPCOOH membrane (compare Fig. 3A and B). This is agreement with the Rg values, where the Cx26 hemichannel embedded into the POPCOOH membrane is more compact, suggesting that lipid oxidation influences the dynamics properties of Cx26 hemichannels. Figure S4 demonstrates that lipid oxidation increases the area per lipid of the lipid bilayer and decreases the bilayer thickness (cf. POPCOOH vs. POPC). Consequently, it will affect the stability and dynamics of the Cx26 hemichannel.

To obtain insights into the interactions between the lipids and the Cx26 hemichannel, we calculated the number of contacts between the center of mass of the headgroups, the double bond, and the –OOH group of lipids with the Cx26 hemichannel (Fig. 4). The lipid headgroups are defined as the phosphate and carbonyl ester groups of each lipid molecule (see Figure S2). Interestingly, we can note slightly less contacts between the center of mass of the headgroups and the double bond of POPCOOH lipids with the hemichannel compared with the number of contacts for POPC lipids (compare Fig. 4A and B), suggesting that POPCOOH lipids are interacting more with each other than with the hemichannel. When calculating the number of hydrogen bonds (H-bonds) between the –OOH group of POPCOOH lipids, with water and other groups of POPCOOH lipids, we can see that the –OOH groups are more prone to establish H-bonds with the carbonyl ester group of POPCOOH lipids around it (Figure S5), which is due to a strong dipole-dipole interaction between these groups. This behavior is in agreement with our previous studies for oxidized membranes, causing a migration of –OOH groups toward the headgroup region and thereby increasing the lipid disorder [82]. Since hemichannels are embedded into the membrane, we can expect that lipid-lipid interactions affect the hemichannel properties. In addition, the –OOH group of POPCOOH lipids is more prone to interact with the hemichannel than the double bond of POPCOOH lipids (see Fig. 4B). In addition, the increase in the area per lipid caused by lipid oxidation (see Figure S4A) will also favor the higher interaction of the –OOH group of POPCOOH lipids with the Cx26 hemichannel (see Fig. 4B).

Altogether, these results suggest that lipid oxidation affects the stability and dynamics of Cx26 hemichannels, and that lipid-lipid and lipid-protein interactions must be taken into account to study the hemichannel properties. It is well known that lipid oxidation increases the membrane permeability [83,84]. In the next section we will discuss the effects of lipid oxidation on the Cx26 hemichannel permeability.

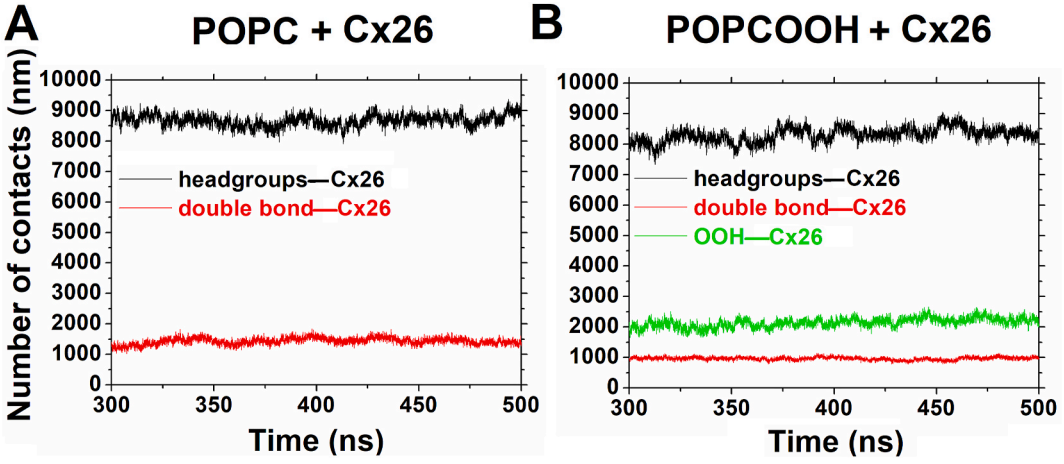

Fig. 4. Number of contacts <0.6 nm between the center of mass of the headgroups, the double bond, and the –OOH group of the lipids and the Cx26 hemichannel embedded into (**A**) the POPC membrane and (**B**) the POPCOOH membrane, calculated from the last 200 ns of simulation.

3.2. Permeability of Cx26 hemichannels

Since lipid oxidation affects the stability and dynamics of the Cx26 hemichannel, we expect it may also affect the hemichannel permeability. In order to evaluate the effect of lipid oxidation on the permeability of the Cx26 hemichannel, we calculated the surface electrostatic potential of the Cx26 hemichannel embedded into either the POPC membrane (Fig. 5) or POPCOOH membrane (Fig. 6). For both systems, we observed a negative surface electrostatic potential near the extracellular side of the hemichannel (red regions) and a positive surface electrostatic potential near the intracellular side (blue regions). We can note that the total electrostatic energy slightly decreases over time when the Cx26 hemichannel is embedded into the POPC membrane (see Fig. 5). Conversely, the total electrostatic energy increases a bit when the Cx26 hemichannel is embedded into the POPCOOH membrane (see Fig. 6).

Changes in the surface electrostatic potential may allow or disrupt the passive diffusion of water, ions, and small molecules across GJs and hemichannels. Indeed, experimental evidence has suggested that the permeability barrier of GJs and hemichannels is modulated by potential differences, through two voltage-regulated gating mechanisms: 1) a transmembrane voltage, i.e., the potential difference between the cytoplasm and the extracellular space; and 2) a transjunctional voltage, i.e., the potential difference between the cytoplasm of two adjacent cells [85,86]. Consequently, an increase in the total electrostatic energy of the Cx26 hemichannel caused by lipid oxidation may affect the hemichannel permeability. For instance, our results demonstrated a higher density of Na^+ ions close to the intracellular and extracellular regions of the Cx26 hemichannel in the presence of native lipids, whereas these Na^+ ions are distributed more homogeneously in the presence of oxidized lipids (compare dark blue lines in Figures S6A and S6B).

To test the hypothesis that changes in the surface electrostatic potential of the Cx26 hemichannel caused by lipid oxidation may affect the hemichannel permeability, we investigated the Cx26 hemichannel pore topology using the Pore-Walker program [73]. Through this tool, we evaluated the average pore diameter profile at different simulation times: 300 ns, 325 ns, 350 ns, 375 ns, 400 ns, 425 ns, 450 ns, 475 ns, and 500 ns (Fig. 7A). The pore diameter profiles at different simulation times can be seen in Figure S7. We calculated the central pore diameter as the narrowest region of the pore diameter profile, i.e., the minimum region. In our simulations, we found a value for the central pore diameter around 9 Å and 8 Å for the Cx26 hemichannel embedded into the POPC membrane and POPCOOH membrane, respectively (see Fig. 7A). Maeda et al. reported a central pore diameter of the Cx26 hemichannel of 14 Å, but their calculation of the central pore diameter was based on minimal center-to-center distances of opposed heavy atoms, and did not consider atom diameters [52]. Thus, our results demonstrate that the central pore diameter of the Cx26 hemichannel is almost the same in the presence of oxidized lipids (see Fig. 7A). Conversely, the pore diameter at the extracellular side of the Cx26 hemichannel is smaller when embedded into the POPCOOH membrane: ca. 16 Å when embedded into the POPCOOH membrane *versus* 21 Å when embedded into the POPC membrane (see Fig. 7A and B), suggesting a more closed conformation of the hemichannel in the presence of oxidized lipids. This more closed conformation is favored by the decrease in the bilayer thickness caused by lipid oxidation (see Figure S4B), thus the hemichannel should constrict to accommodate in the membrane. The decrease in the bilayer thickness is correlated with membrane pore formation [83] and may affect lipid-protein interactions, such as the stability/activity of the Cx26 hemichannel. The closed conformation of the Cx26 hemichannel embedded into the POPCOOH membrane was also observed when analyzing the Cx26 hemichannel density maps: we can note that the pore diameter at the extracellular side is smaller in the presence of oxidized lipids (compare Fig. 8A and B).

Moreover, our results also demonstrate that the pore diameter at the NT domains is larger for the Cx26 hemichannel embedded into the POPCOOH membrane: ca. 22 Å when embedded into the POPCOOH membrane *versus* 19 Å when embedded into the POPC membrane (see Fig. 7A). Experimental evidence has suggested that the NT domains participate in the voltage-regulated gating mechanism of hemichannels and GJs, moving in response to changes in electrical potential [87,88]. Thus, to obtain a quantitative measure of the effect of the NT domains on the hemichannel pore, we introduced a parameter, called eccentricity coefficient (*E*), defined as the ratio between the maximum and minimum diameter of a hexagon built on the Cα of the six asparagine amino acid residues within the NT domains that compose the Cx26 hemichannel (see Figure S8 for more details). We computed *E* values equal to 1.391 ± 0.303 and 1.436 ± 0.152 for the Cx26 hemichannel embedded into the POPC membrane and the POPCOOH membrane, respectively. Therefore, the Cx26 hemichannel pore at the NT domains is slightly larger in diameter when it is embedded into oxidized membranes. Note that these values are higher than the *E* value found by Zonta et al. [89] for the uncompleted crystal structure of the Cx26 hemichannel (i.e., 1.10 ± 0.05), suggesting that the missing amino acids residues in the

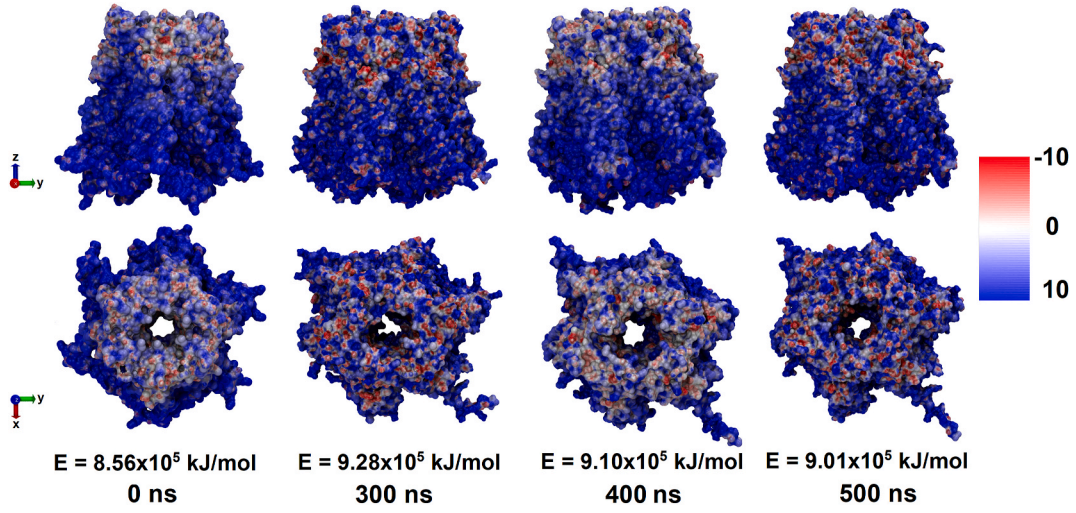

Fig. 5. Surface electrostatic potential of the Cx26 hemichannel embedded into the POPC membrane, calculated with the adaptive Poisson-Boltzmann solver (APBS) program. Red colours represent negative charges, and blue colours positive charges. The colour scale represents the range of the average charges. The *E* values represent the total electrostatic energy. The solute and solvent dielectrics are 2.000 and 78.540, respectively. The solvent probe radius is 1.400 Å and the temperature is 298.150 K.

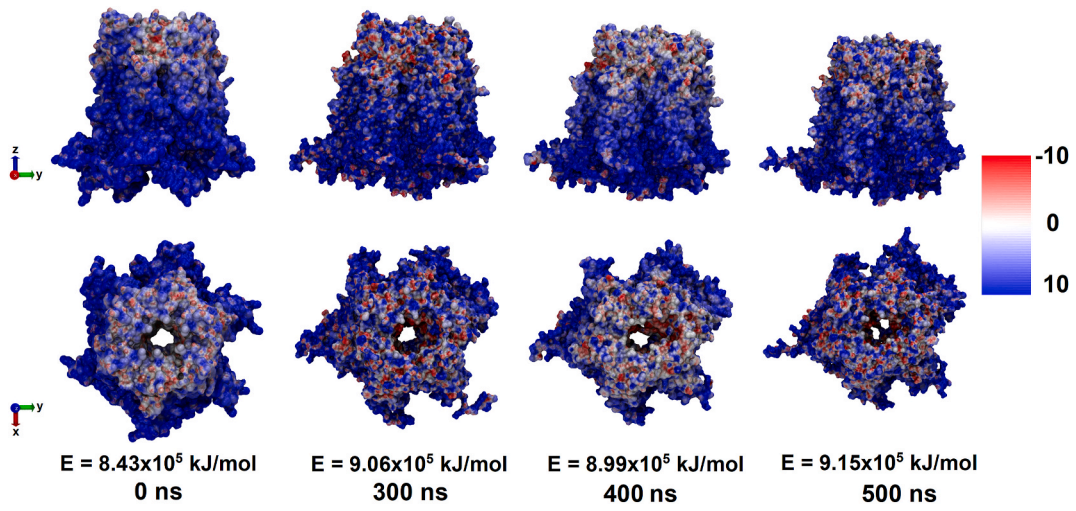

Fig. 6. Surface electrostatic potential of the Cx26 hemichannel embedded into the POPCOOH membrane, calculated with the adaptive Poisson-Boltzmann solver (APBS) program. Red colours represent negative charges, and blue colours positive charges. The colour scale represents the range of the average charges. The *E* values represent the total electrostatic energy. The solute and solvent dielectrics are 2.000 and 78.540, respectively. The solvent probe radius is 1.400 Å and the temperature is 298.150 K.

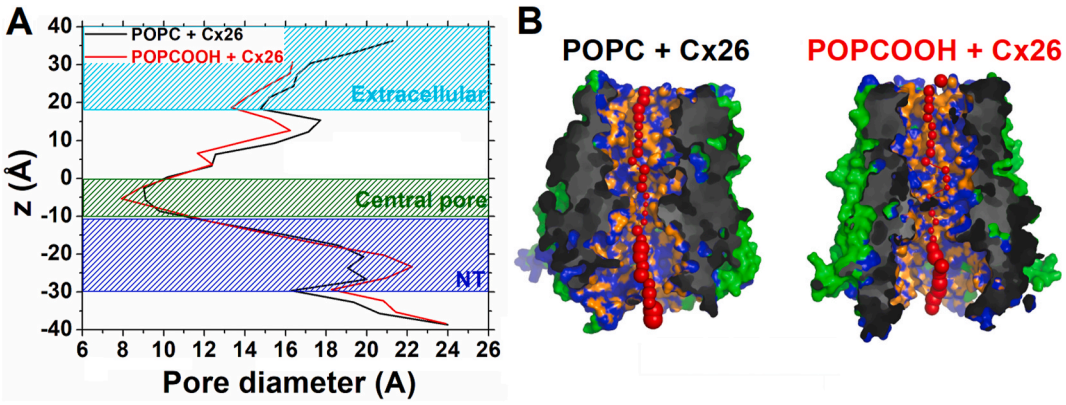

Fig. 7. Characterization of the Cx26 hemichannel embedded into POPC and POPCOOH membranes, calculated with Pore-Walker. (**A**) Average pore diameter profile at 3 Å steps. (**B**) Visualization of pore section showing the position of the pore centers (red spheres) at 500 ns of simulation time. The red spheres are proportional to the corresponding measured diameters, i.e., 1/10 of the pore diameter calculated at that point. Pore-lining atoms and amino acid residues are coloured in orange and blue, respectively. The remaining part of the protein is shown in green and black.

uncompleted crystal structure are important to evaluate the channel gating properties of the Cx26 hemichannel.

We also analyzed the dynamical behavior of the NT domains by tracking the angles (*A*) of the hexagon built on the Cα of the six threonine amino acid residues within the NT domains that compose the Cx26 hemichannel (see Figure S8 for more details). In Figure S9 we plot the temporal evolution of the angles in the Cx26 hemichannel embedded into the POPC membrane and the POPCOOH membrane. Note that the Cx26 hemichannel embedded into the POPCOOH membrane displays larger angle variations than when it is embedded into the POPC membrane (compare Figures S9A and S9B). This angle analysis is in agreement with our calculated *E* values, where lipid oxidation slightly increases the pore diameter at the NT domains of the Cx26 hemichannel. It should be pointed out that although the difference between our calculated *E* values for the Cx26 hemichannel embedded into the POPC membrane and the POPCOOH membrane is very small, we must pay attention to how lipid oxidation influences the Cx26 hemichannel properties, instead of their absolute values. In addition, the difference between our calculated *E* values is more significant looking at the angle variations of the hexagon (see Figure S9).

We further analyzed how lipid oxidation affects not only the pore diameter profile, but also the physical chemical properties, such as polarity and charge at different pore length and radius, using the MOLEonline program [74]. For both systems, we observe an increase in the polarity at the extra- and intracellular sides of the Cx26 hemichannel (Figures S10 and S11). However, the presence of oxidized lipids increases the polarity in the transmembrane region of the Cx26 hemichannel (compare Figures S10 and S11). Hence, it may facilitate the passage of polar molecules. Indeed, the water density at the transmembrane region of the Cx26 hemichannel is slightly higher in the presence of oxidized lipids (Fig. 9A). Likewise, the ΔG for water permeation across the Cx26 hemichannel is overall slightly lower at the transmembrane region in the presence of oxidized lipids (Fig. 9B). These results strengthen the idea that lipid oxidation slightly increases the permeability of the Cx26 hemichannel.

3.3. Distribution and dynamics of RONS over the Cx26 hemichannel

To evaluate the permeability of the Cx26 hemichannel more in-depth, we also performed equilibrium simulations of RONS distributed over the Cx26 hemichannel embedded into either a POPC membrane or a POPCOOH membrane, in order to verify whether RONS may permeate

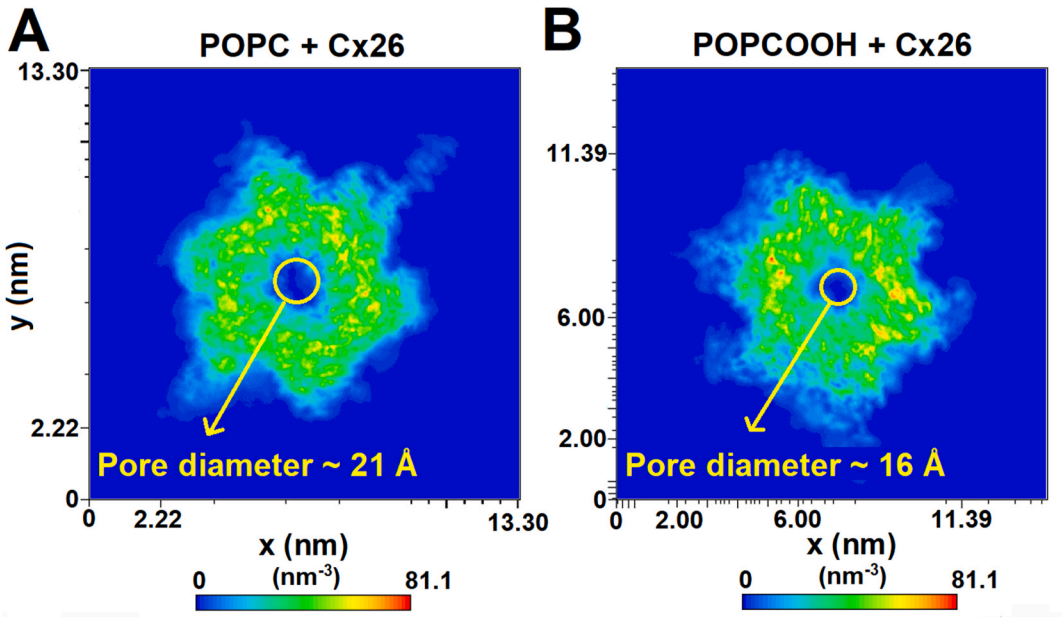

Fig. 8. Density maps of the Cx26 hemichannel embedded into (**A**) the POPC membrane and (**B**) the POPCOOH membrane, calculated from the last 200 ns of simulation. The dark blue region corresponds to the absence of protein (space occupied by the lipids). The yellow circle represents the pore diameter at the extracellular side, calculated in Fig. 7A.

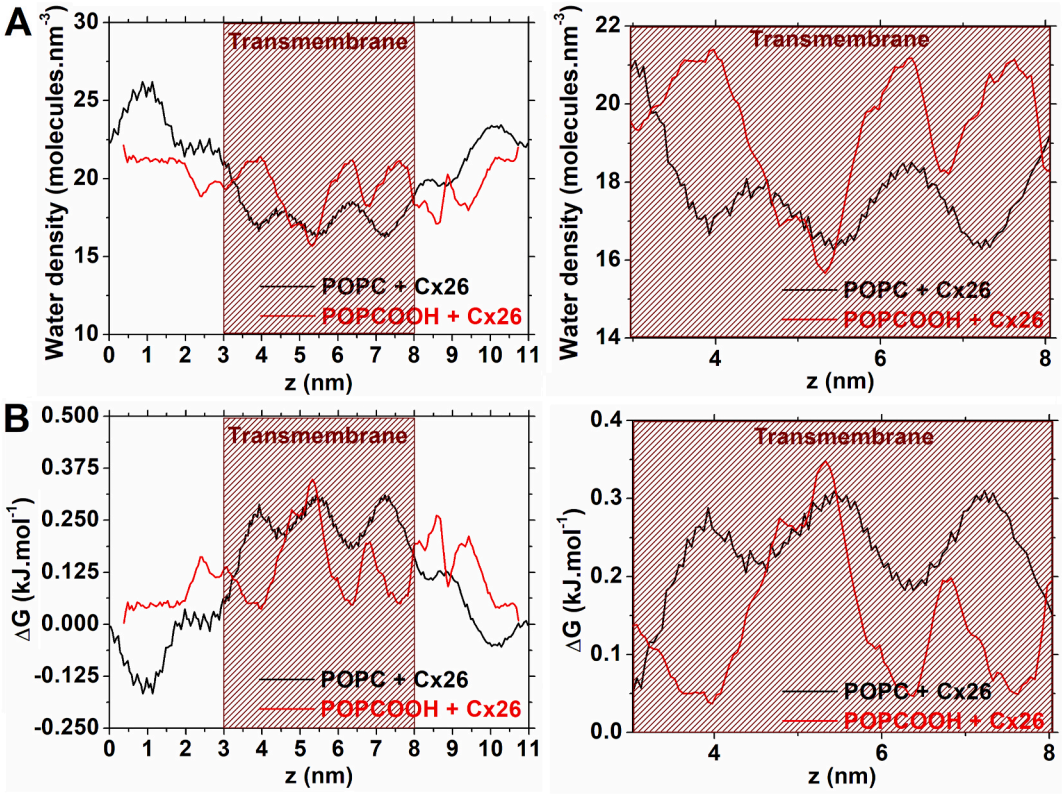

Fig. 9. Analysis of water permeation across the Cx26 hemichannel, calculated from the last 200 ns of simulation: (**A**) Distribution of water molecules along the Cx26 hemichannel (left) and expansion of the transmembrane regions (right); and (**B**) Free energy (ΔG) for water permeation across the Cx26 hemichannel (left) and expansion of the transmembrane regions (right). The position $z = 5.25$ nm was set at the central pore region.

the Cx26 hemichannel easier in the presence of oxidized membranes. It is important to understand the distribution and dynamics of RONS at hemichannels, since RONS can modulate the GJ and hemichannel activity [37,90]. For instance, Xu et al. performed reactive MD simulations of the Cx26 hemichannel reacting with $HO^{\bullet}$ and $HO_2^{\bullet}$ radicals, and they found that these radicals chemically react with the NT domains of the Cx26 hemichannel, and can structurally damage the Cx26 hemichannel [91].

Thus, we studied the behavior of RONS starting at the water/lipid interface, and how they can permeate the membrane in the presence of

the Cx26 hemichannel. For this purpose, 200 $HO_2^{\bullet}$ radicals were initially placed together in the aqueous phase (100 molecules in the upper aqueous phase and 100 in the bottom aqueous phase), surrounding a pre-equilibrated model system of the Cx26 hemichannel embedded into either a POPC membrane or a POPCOOH membrane. This value corresponds to an initial molar fraction of ca. 0.5% for each $HO_2^{\bullet}$ radical in the aqueous phase, which is several orders of magnitude higher than the experimentally measured RONS concentrations in mitochondria [92] but it is needed to obtain reasonable statistics. We chose these RONS based on the work of Xu et al. [91] and the similarity with the –OOH group attached to POPC lipid molecules (oxidized lipids).

Fig. 10 shows the trajectory of the $HO_2^{\bullet}$ radicals from the last 50 ns of simulation. At first glance, most of the $HO_2^{\bullet}$ radicals remain at the water/lipid interface when the Cx26 hemichannel is embedded into the POPC membrane (see Fig. 10A). On the other hand, most of these radicals permeate the Cx26 hemichannel in the presence of oxidized lipids (see Fig. 10B), suggesting a higher interaction of the $HO_2^{\bullet}$ radicals with the hemichannel.

We calculated the radial distribution function (RDF) of the $HO_2^{\bullet}$ radicals for each domain of the Cx26 hemichannel, and our results demonstrate that indeed these radicals interact more with the TM domains of the Cx26 hemichannel embedded in a POPCOOH membrane (compare red, orange, green, and purple lines in Fig. 11). Additionally, these radicals also establish more interactions with the NT domains of the Cx26 hemichannel embedded into the POPCOOH membrane (compare blue lines in Fig. 11). Specifically, the $HO_2^{\bullet}$ radicals are more prone to interact with the asparagine Asp_2 and glutamine Gln_7 amino acid residues of the NT domains: When calculating the minimum distances between $HO_2^{\bullet}$ radicals and each amino acid residue of the NT domains of the Cx26 hemichannel embedded into the POPCOOH membrane, we found that these radicals present a somewhat shorter distance to Asp_2 and Gln_7 amino acid residues (Table S2). In Figure S12 we can see the interaction between the $HO_2^{\bullet}$ radicals and the NT domains of the Cx26 hemichannel embedded into the POPCOOH membrane. These analyses support the idea that RONS may permeate easier the Cx26 hemichannel in the presence of oxidized lipids.

The ability of GJs to enhance the intracellular accumulation of RONS has been widely explored experimentally [40,93,94]. For instance, Wu et al. demonstrated that Cx26-GJs increased the level of intracellular RONS in HeLa cells treated with PDT [40], suggesting that GJs may improve the sensitivity of cancer cells to PDT-induced cell death. Cx26 hemichannels were also found to be able to improve PDT treatment by bystander cell killing [38]. Concurrently, Cx43-composed GJ channels (Cx43-GJs) also increased the sensitivity of melanoma cells to RONS during non-thermal plasma (NTP) treatment, and propagated apoptotic death signals to neighbouring cells (bystander effect) [95]. These results highlight the property of GJs to enhance oxidative stress-induced cell death during cancer treatments, based on e.g., PDT and NTP, but it can also be applicable to other treatments based on oxidative stress. In addition, since mutations in Cx26, Cx30, Cx31, Cx32, and Cx43 proteins have been associated with nonsyndromic or syndromic deafness in humans [96–98], the oxidative damage induced by oxidative stress may affect Cx proteins-mediated deafness and hearing loss [99].

Our results for the distribution and dynamics of $HO_2^{\bullet}$ radicals over the Cx26 hemichannel reinforce the idea that Cx26 hemichannels could enhance the intracellular accumulation of RONS in cancer cells during oxidative stress-based treatments, and this effect may be stronger in the presence of oxidized lipids. However, additional studies are still necessary to elucidate the mechanism of RONS transportation through GJs and hemichannels. Calculation of the free energy profiles for RONS permeation across the Cx26 hemichannel by means of equilibrium simulations would require unrealistically high concentrations of these

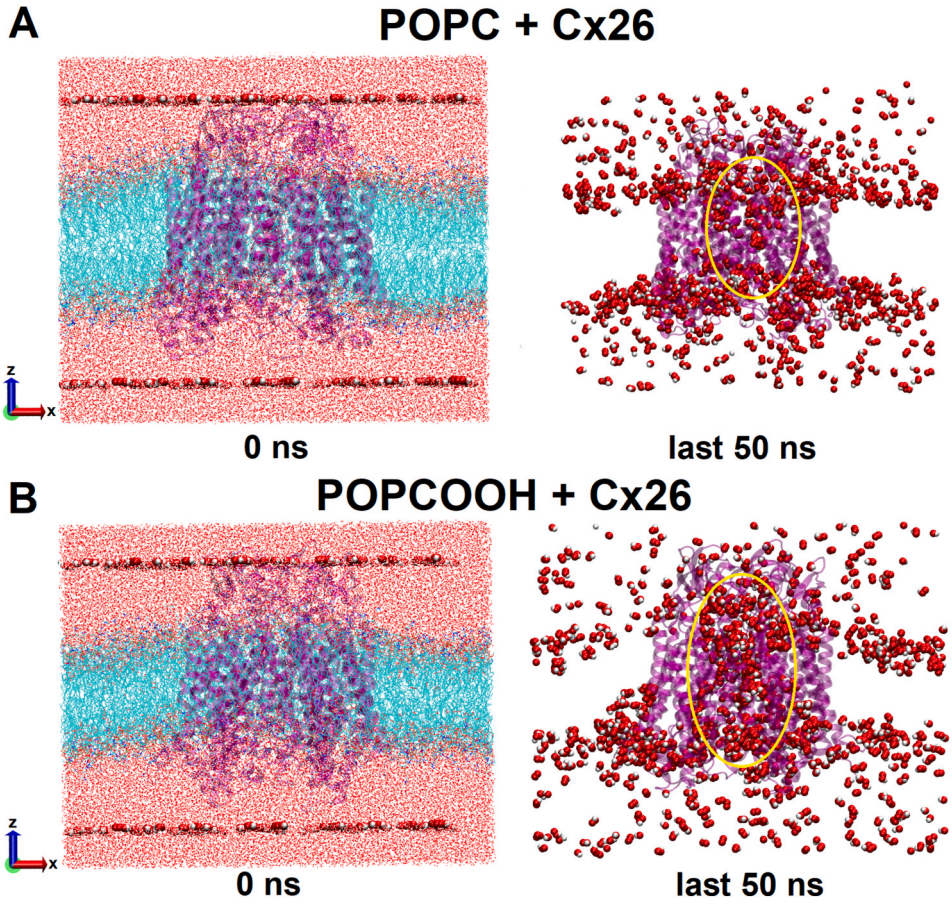

Fig. 10. Snapshot of the initial structure (left) and trajectory of the last 50 ns (right) of the equilibrium simulations of $HO_2^{\bullet}$ radicals over the Cx26 hemichannel embedded into (**A**) the POPC membrane and (**B**) the POPCOOH membrane. Lipid molecules are represented as lines of different colours, water molecules as red points, the Cx26 hemichannel as shadow ribbons, and the $HO_2^{\bullet}$ radicals as red and white van der Waals spheres. For the sake of clarity, lipids and water molecules are not represented in the trajectory (i.e., last 50 ns). All frames of the last 50 ns are overlaid in order to highlight the permeation path of $HO_2^{\bullet}$ radicals (only $HO_2^{\bullet}$ radicals within 0.4 nm of the Cx26 hemichannel are represented). We can see that the $HO_2^{\bullet}$ radicals remain more at the water/lipid interface in case of the POPC membrane, while they interact more with the Cx26 hemichannel in the case of the POPCOOH membrane. The yellow circles represent the $HO_2^{\bullet}$ radicals that permeate the Cx26 hemichannel pore.

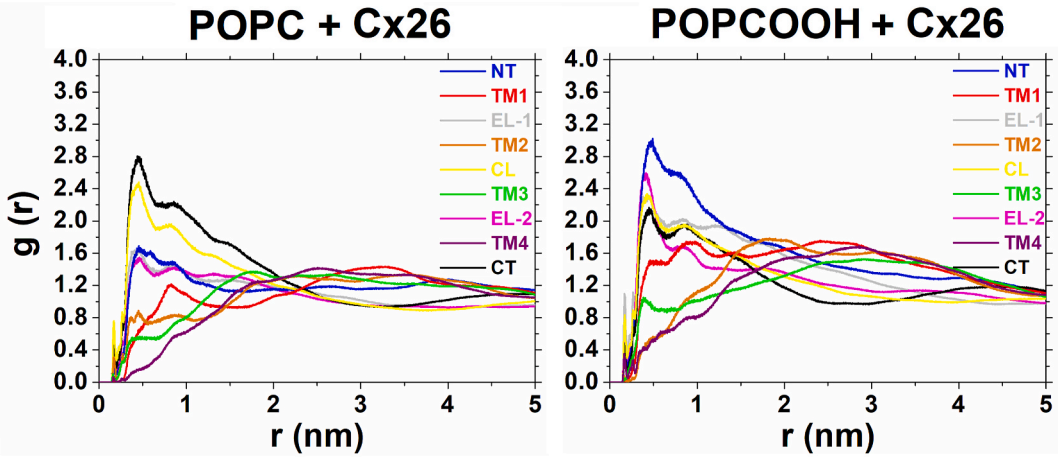

Fig. 11. Radial distribution function (RDF) of $HO_2^{\bullet}$ radicals calculated from the last 50 ns of simulation, for Cx26 embedded into POPC and POPCOOH membranes. The RDFs of the $HO_2^{\bullet}$ radicals are generally higher in the latter case, indicating that these radicals stronger interact with the Cx26 hemichannel when embedded into the POPCOOH membrane.

species in solution. This could lead to artifacts in solvent properties and hemichannel conformation. Therefore, more accurate techniques should be used, such as umbrella sampling simulations [100]. We will address this issue in our future work.

4. Conclusions

The dual property of GJs and Cxs to act as tumor suppressors or tumor promoters allows us to modulate these properties in cancer cells, to hinder cancer progression. Modulation of these properties can assist the activation of anti-cancer immunity, propagation of cell death, and oxidative stress-mediated cell death [101]. One promising therapeutic strategy is the use of these GJ channels to transport RONS to the interior of cancer cells, and kill them by oxidative stress. However, little is known about the mechanism of RONS transportation across GJs and hemichannels. In addition, the effect of lipid oxidation on the properties of GJs and hemichannels still needs to be elucidated. In this work, we studied how RONS-induced lipid oxidation affects the channel properties of Cx26 hemichannels. Our simulation results demonstrate that lipid oxidation induces changes in the stability and dynamics of Cx26 hemichannels, affecting lipid-lipid and lipid-protein interactions. Interestingly, the presence of oxidized lipids changes the pore diameter profile of the Cx26 hemichannel: the pore diameter decreases at the extracellular side and increases at the NT domains. Since the NT domains are strongly correlated to the gating mechanisms of hemichannels and GJs, a larger pore diameter would improve the entry and accumulation of RONS inside the cell to cause oxidative damage. Indeed, our simulations demonstrate that $HO_2^{\bullet}$ radicals are more prone to interact with the TM and NT domains of the Cx26 hemichannel in the presence of oxidized lipids, strengthening the idea that lipid oxidation facilitates the intracellular accumulation of RONS through the hemichannel. Our results are in agreement with experimental results for other Cx hemichannels (e.g., Cx46 hemichannels) where lipid oxidation affected the hemichannel activity [13,42]. Our results highlight lipid oxidation as an important factor to be considered when modulating GJ properties during oxidative stress-mediated cell death. A better understanding of these effects may improve the efficacy of oxidative stress-based cancer treatments, such as e.g., PDT and NTP.

It should be pointed out that the number of atoms of GJ channels (>500,000) restricts full atomistic MD simulations of these systems to a couple of hundreds of nanoseconds, and this simulation time might be insufficient to obtain an equilibrated and fully open GJ channel, given its size and complexity. However, independently whether our equilibrated Cx26 hemichannel is in its open or closed conformation, our results demonstrate that lipid oxidation affects the channel properties of Cx26 hemichannels. Additionally, given the permeability of hemichannels for a large variety of physiological signaling molecules, we will consider exploring in future studies the permeability of ATP, glutamate and other signaling molecules, across Cx26 hemichannels in the presence of oxidized lipids.

Declarations of interest

None.

Acknowledgment

We thank the University of Antwerp and the Turing HPC infrastructure at the CalcUA core facility of the University of Antwerp, a division of the Flemish Supercomputer Center VSC, funded by the Hercules Foundation, the Flemish Government (department EWI), for providing the computational resources needed for running the simulations. This work was funded by the Research Foundation-Flanders (FWO), project number 42/FA070200/8300.

Appendix A. Supplementary data

Supplementary data related to this article can be found at https://doi.org/10.1016/j.abb.2023.109741.

References

[1] E. Armingol, A. Officer, O. Harismendy, N.E. Lewis, Deciphering cell–cell interactions and communication from gene expression, Nat. Rev. Genet. 22 (2021) 71–88.
[2] Q. Wei, H. Huang, Chapter five - insights into the role of cell–cell junctions in physiology and disease, Int. Rev. Cell Mol. Biol. 306 (2013) 187–221.
[3] M. Vinken, Introduction: connexins, pannexins and their channels as gatekeepers of organ physiology, Cell. Mol. Life Sci. 72 (2015) 2775–2778.
[4] D.A. Goodenough, D.L. Paul, Gap junctions, Cold Spring Harbor Perspect. Biol. 1 (2009) 1–19.
[5] W.H. Evans, Cell communication across gap junctions: a historical perspective and current developments, Biochem. Soc. Trans. 43 (2015) 450–459.
[6] M. Oyamada, K. Takebe, Y. Oyamada, Regulation of connexin expression by transcription factors and epigenetic mechanisms, Biochim. Biophys. Acta Biomembr. 1828 (2013) 118–133.
[7] R.T. Mathias, T.W. White, X. Gong, Lens gap junctions in growth, differentiation, and homeostasis, Physiol. Rev. 90 (2010) 179–206.
[8] T. Okamoto, H. Usuda, T. Tanaka, K. Wada, M. Shimaoka, The functional implications of endothelial gap junctions and cellular mechanics in vascular angiogenesis, Cancers 11 (2019) 237.
[9] G.Y. Huang, E.S. Cooper, K. Waldo, M.L. Kirby, N.B. Gilula, C.W. Lo, Gap junction–mediated cell–cell communication modulates mouse neural crest migration, J. Cell Biol. 143 (1998) 1725–1734.

[10] Q. Peng, C. Yue, A.C.H. Chen, K.C. Lee, S.W. Fong, W.S.B. Yeung, Y.L. Lee, Connexin 43 is involved in early differentiation of human embryonic stem cells, Differentiation 105 (2019) 33–44.
[11] M.A. Retamal, S. Yin, G.A. Altenberg, L. Reuss, Voltage-dependent facilitation of Cx46 hemichannels, Am. J. Physiol. Cell Physiol. 298 (2010) C132–C139.
[12] X. Bao, G.A. Altenberg, L. Reuss, Mechanism of regulation of the gap junction protein connexin 43 by protein kinase C-mediated phosphorylation, Am. J. Physiol. Cell Physiol. 286 (2004) C647–C654.
[13] M.A. Retamal, F. Evangelista-Martínez, C.G. León-Paravic, G.A. Altenberg, L. Reuss, Biphasic effect of linoleic acid on connexin 46 hemichannels, Pflügers Archiv 461 (2011) 635–643.
[14] M.A. Retamal, S. Yin, G.A. Altenberg, L. Reuss, Modulation of Cx46 hemichannels by nitric oxide, Am. J. Physiol. Cell Physiol. 296 (2009) C1356–C1363.
[15] V.A. Skeberdis, L. Rimkute, A. Skeberdyte, N. Paulauskas, F.F. Bukauskas, pH-dependent modulation of connexin-based gap junctional uncouplers, J. Physiol. 589 (2011) 3495–3506.
[16] W. Lopez, Y. Liu, A.L. Harris, J.E. Contreras, Divalent regulation and intersubunit interactions of human connexin26 (Cx26) hemichannels, Channels 8 (2014) 1–4.
[17] M.G. Tejada, S. Sudhakar, N.K. Kim, H. Aoyama, B.H. Shilton, D. Bai, Variants with increased negative electrostatic potential in the Cx50 gap junction pore increased unitary channel conductance and magnesium modulation, Biochem. J. 475 (2018) 3315–3330.
[18] M.A. Retamal, G.A. Altenberg, Role and posttranslational regulation of Cx46 hemichannels and gap junction channels in the eye lens, Front. Physiol. 13 (2022), 864948.
[19] P.L. Sorgen, A.J. Trease, G. Spagnol, M. Delmar, M.S. Nielsen, Protein–protein interactions with connexin 43: regulation and function, Int. J. Mol. Sci. 19 (2018) 1428.
[20] J. Gilleron, D. Carette, D. Chevallier, D. Segretain, G. Pointis, Molecular connexin partner remodeling orchestrates connexin traffic: from physiology to pathophysiology, Crit. Rev. Biochem. Mol. Biol. 47 (2012) 407–423.
[21] M.M. Falk, C.L. Bell, R.M.K. Andrews, S.A. Murray, Molecular mechanisms regulating formation, trafficking and processing of annular gap junctions, BMC Cell Biol. 17 (2016) 22.
[22] J.L. Solan, P.D. Lampe, Spatio-temporal regulation of connexin43 phosphorylation and gap junction dynamics, Biochim. Biophys. Acta Biomembr. 1860 (2018) 83–90.
[23] H. Yamasaki, V. Krutovskikh, M. Mesnil, T. Tanaka, M.L. Zaidan-Dagli, Y. Omori, Role of connexin (gap junction) genes in cell growth control and carcinogenesis, C. R. Acad. des Sci. Paris, Sciences de la vie/Life Sciences 322 (1999) 151–159.
[24] H. Lahlou, M. Fanjul, L. Pradayrol, C. Susini, S. Pyronnet, Restoration of functional gap junctions through internal ribosome entry site-dependent synthesis of endogenous connexins in density-inhibited cancer cells, Mol. Cell Biol. 25 (2005) 4034–4045.
[25] I. Teleki, A.M. Szasz, M.E. Maros, B. Gyorffy, J. Kulka, N. Meggyeshazi, G. Kiszner, P. Balla, A. Samu, T. Krenacs, Correlations of differentially expressed gap junction connexins Cx26, Cx30, Cx32, Cx43 and Cx46 with breast cancer progression and prognosis, PLoS One 9 (2014), e112541.
[26] M. Hitomi, L.P. Deleyrolle, E.E. Mulkearns-Hubert, A. Jarrar, M. Li, M. Sinyuk, B. Otvos, S. Brunet, W.A. Flavahan, C.G. Hubert, W. Goan, J.S. Hale, A. G. Alvarado, A. Zhang, M. Rohaus, M. Oli, V. Vedam-Mai, J.M. Fortin, H.S. Futch, B. Griffith, Q. Wu, C.-H. Xia, X. Gong, M.S. Ahluwalia, J.N. Rich, B.A. Reynolds, J. D. Lathia, Differential connexin function enhances self-renewal in glioblastoma, Cell Rep. 11 (2015) 1031–1042.
[27] M. Mesnil, S. Crespin, J.L. Avanzo, M.L. Zaidan-Dagli, Defective gap junctional intercellular communication in the carcinogenic process, Biochim. Biophys. Acta Biomembr. 1719 (2005) 125–145.
[28] C. Moorby, M. Patel, Dual functions for connexins: Cx43 regulates growth independently of gap junction formation, Exp. Cell Res. 271 (2001) 238–248.
[29] T.K. Nelson, P.L. Sorgen, J.M. Burt, Carboxy terminus and pore-forming domain properties specific to Cx37 are necessary for Cx37-mediated suppression of insulinoma cell proliferation, Am. J. Physiol. Cell Physiol. 305 (2013) C1246–C1256.
[30] S. Fukuda, M. Akiyama, Y. Niki, R. Kawatsura, H. Harada, K.-I. Nakahama, Inhibitory effects of miRNAs in astrocytes on C6 glioma progression via connexin 43, Mol. Cell. Biochem. 476 (2021) 2623–2632.
[31] K. Stoletov, J. Strnadel, E. Zardouzian, M. Momiyama, F.D. Park, J.A. Kelber, D. P. Pizzzo, R. Hoffman, S.R. VandenBerg, R.L. Klemke, Role of connexins in metastatic breast cancer and melanoma brain colonization, J. Cell Sci. 126 (2013) 904–913.
[32] J.-I. Wu, L.-H. Wang, Emerging roles of gap junction proteins connexins in cancer metastasis, chemoresistance and clinical application, J. Biomed. Sci. 26 (2019) 8.
[33] I.E. García, P. Prado, A. Pupo, O. Jara, D. Rojas-Gómez, P. Mujica, C. Flores-Muñoz, J. González-Casanova, C. Soto-Riveros, B.I. Pinto, M.A. Retamal, C. González, A.D. Martínez, Connexinopathies: a structural and functional glimpse, BMC Cell Biol. 17 (2016) S17.
[34] M. Srinivas, V.K. Verselis, T.W. White, Human diseases associated with connexin mutations, Biochim. Biophys. Acta Biomembr. 1860 (2018) 192–201.
[35] M. Valko, D. Leibfritz, J. Moncol, M.T.D. Cronin, M. Mazur, J. Telser, Free radicals and antioxidants in normal physiological functions and human disease, Int. J. Biochem. Cell Biol. 39 (2007) 44–84.
[36] C.M.L. Hutnik, C.E. Pocrnich, H. Liu, D.W. Laird, Q. Shao, The protective effect of functional Connexin43 channels on a human epithelial cell line exposed to oxidative stress, Invest. Ophthalmol. Vis. Sci. 49 (2008) 800–806.
[37] Y.-M. Quan, Y. Du, C.-G. Wu, S. Gu, J.X. Jiangb, Connexin hemichannels regulate redox potential via metabolite exchange and protect lens against cellular oxidative damage, Redox Biol. 46 (2021), 102102.
[38] C. Nardin, C. Peres, S. Putti, T. Orsini, C. Colussi, F. Mazzarda, M. Raspa, F. Scavizzi, A.M. Salvatore, F. Chiani, A. Tettey-Matey, Y. Kuang, G. Yang, M. A. Retamal, F. Mammano, Connexin hemichannel activation by S-nitrosoglutathione synergizes strongly with photodynamic therapy potentiating anti-tumor bystander killing, Cancers 13 (2021) 5062.
[39] T. Yamaguchi, M. Yoneyama, E. Hinoi, K. Ogita, Involvement of calpain in 4-hydroxynonenal-induced disruption of gap junction-mediated intercellular communication among fibrocytes in primary cultures derived from the cochlear spiral ligament, J. Pharmaceut. Sci. 129 (2015) 127–134.
[40] D.-P. Wu, T.-Y. Lin, L.-R. Bai, J.-L. Huang, Y. Zhou, N. Zhou, S.-L. Zhong, S. Gao, X.-X. Yin, Enhanced phototoxicity of photodynamic treatment by Cx26-composed GJIC via ROS-, calcium- and lipid peroxide-mediated pathways, J. Biophot. 10 (2017) 1586–1596.
[41] B.E. Isakson, G. Kronke, A. Kadl, N. Leitinger, B.R. Duling, Oxidized phospholipids alter vascular connexin expression, phosphorylation, and heterocellular communication, Arterioscler. Thromb. Vasc. Biol. 26 (2006) 2216–2221.
[42] M.A. Retamal, Carbon monoxide modulates connexin function through a lipid peroxidation-dependent process: a hypothesis, Front. Physiol. 7 (2016) 259.
[43] M. Mosca, A. Ceglie, L. Ambrosone, Effect of membrane composition on lipid oxidation in liposomes, Chem. Phys. Lipids 164 (2011) 158–165.
[44] I.O.L. Bacellar, M.S. Baptista, Mechanisms of photosensitized lipid oxidation and membrane permeabilization, ACS Omega 4 (2019) 21636–21646.
[45] E. Parra-Ortiz, K.L. Browning, L.S.E. Damgaard, R. Nordström, S. Micciulla, S. Bucciarelli, M. Malmsten, Effects of oxidation on the physicochemical properties of polyunsaturated lipid membranes, J. Colloid Interface Sci. 538 (2019) 404–419.
[46] P. Siani, R.M. de Souza, L.G. Dias, R. Itri, H. Khandelia, An overview of molecular dynamics simulations of oxidized lipid systems, with a comparison of ELBA and MARTINI force fields for coarse grained lipid simulations, Biochim. Biophys. Acta Biomembr. 1858 (2016) 2498–2511.
[47] D. Wiczew, N. Szulc, M. Tarek, Molecular dynamics simulations of the effects of lipid oxidation on the permeability of cell membranes, Bioelectrochemistry 141 (2021), 107869.
[48] H. Aceves-Luna, D. Glossman-Mitnik, N. Flores-Holguín, Oxidation degree of a cell membrane model and its response to structural changes, a coarse-grained molecular dynamics approach, J. Biomol. Struct. Dyn. 40 (2022) 1930–1941.
[49] A. Adak, Y.C. Unal, S. Yucel, Z. Vural, F.B. Turan, O. Yalcin-Ozuysal, E. Ozcivici, G. Mese, Connexin 32 induces pro-tumorigenic features in MCF10A normal breast cells and MDA-MB-231 metastatic breast cancer cells, Biochim. Biophys. Acta, Mol. Cell Res. 1867 (2020), 118851.
[50] T. Aasen, I. Sansano, M.Á. Montero, C. Romagosa, J. Temprana-Salvador, A. Martínez-Marti, T. Moliné, J. Hernández-Losa, S.R. y Cajal, Insight into the role and regulation of gap junction genes in lung cancer and identification of nuclear Cx43 as a putative biomarker of poor prognosis, Cancers 11 (2019) 320.
[51] R.A. Acuña, M. Varas-Godoy, D. Herrera-Sepulveda, M.A. Retamal, Connexin46 expression enhances cancer stem cell and epithelial-to-mesenchymal transition characteristics of human breast cancer MCF-7 cells, Int. J. Mol. Sci. 22 (2021), 12604.
[52] S. Maeda, S. Nakagawa, M. Suga, E. Yamashita, A. Oshima, Y. Fujiyoshi, T. Tsukihara, Structure of the connexin 26 gap junction channel at 3.5 Å resolution, Nature 458 (2009) 597–602.
[53] T. Kwon, A.L. Harris, A. Rossi, T.A. Bargiello, Molecular dynamics simulations of the Cx26 hemichannel: evaluation of structural models with Brownian dynamics, J. Gen. Physiol. 138 (2011) 475–493.
[54] J.M.R. Albano, N. Mussini, R. Toriano, J.C. Facelli, M.B. Ferraro, M. Pickholz, Calcium interactions with Cx26 hemmichannel: spatial association between MD simulations biding sites and variant pathogenicity, Comput. Biol. Chem. 77 (2018) 331–342.
[55] G. van Meer, D. R Voelker, G.W. Feigenson, Membrane lipids: where they are and how they behave, Nat. Rev. Mol. Cell Biol. 9 (2008) 112–124.
[56] N. Kucerka, J.D. Perlmutter, J. Pan, S. Tristram-Nagle, J. Katsaras, J.N. Sachs, The effect of cholesterol on short- and long-chain monounsaturated lipid bilayers as determined by molecular dynamics simulations and X-ray scattering, Biophys. J. 95 (2008) 2792–2805.
[57] A.W. Girotti, Photosensitized oxidation of membrane lipids: reaction pathways, cytotoxic effects, and cytoprotective mechanisms, J. Photochem. Photobiol. B Biol. 63 (2001) 103–113.
[58] C. Kandt, W.L. Ash, D.P. Tieleman, Setting up and running molecular dynamics simulations of membrane proteins, Methods 41 (2007) 475–488.
[59] W.K. Subczynski, M. Pasenkiewicz-Gierula, J. Widomska, L. Mainali, M. Raguz, High cholesterol/low cholesterol: effects in biological membranes: a review, Cell Biochem. Biophys. 7 (2017) 369–385.
[60] M.J. Abraham, T. Murtola, R. Schulz, S. Pall, J.C. Smith, B. Hess, E. Lindahl, GROMACS: high performance molecular simulations through multi-level parallelism from laptops to super-computers, Software 1–2 (2015) 19–25.
[61] N. Schmid, A.P. Eichenberger, A. Choutko, S. Riniker, M. Winger, A.E. Mark, W. F. van Gunsteren, Definition and testing of the GROMOS force-field versions 54A7 and 54B7, Eur. Biophys. J. 40 (2011) 843–856.
[62] D. Poger, A.E. Mark, On the validation of molecular dynamics simulations of saturated and cis-monounsaturated phosphatidylcholine lipid bilayers: a comparison with experiment, J. Chem. Theor. Comput. 6 (2010) 325–336.

[63] A.J.P. Neto, R.M. Cordeiro, Molecular simulations of the effects of phospholipid and cholesterol peroxidation on lipid membrane properties, Biochim. Biophys. Acta Biomembr. 1858 (2016) 2191–2198.
[64] H.J.C. Berendsen, J.P.M. Postma, W.F. van Gunsteren, J. Hermans, Interaction models for water in relation to protein hydration, in: Intermolecular Forces, B. Pullman, Dordrecht, 1981, pp. 331–342.
[65] I.G. Tironi, A generalized reaction field method for molecular dynamics simulations, J. Chem. Phys. 102 (1995) 5451.
[66] B. Hess, H. Bekker, H.J.C. Berendsen, J.G.E.M. Fraaije, LINCS: a linear constraint solver for molecular simulations, J. Comput. Chem. 18 (1997) 1463–1472.
[67] S. Nose, A molecular-dynamics method for simulations in the canonical ensemble, Mol. Phys. 52 (1984) 255–268.
[68] W.G. Hoover, Canonical dynamics - equilibrium phase-space distributions, Phys. Rev. A: At., Mol., Opt. Phys. 31 (1985) 1695–1697.
[69] M. Parrinello, A. Rahman, Polymorphic Transitions in Single-Crystals- A new molecular-dynamics method, J. Appl. Phys. 52 (1981) 7182–7190.
[70] A. Raudino, F. Zuccarello, C. La Rosa, G. Buemi, Thermal expansion and compressibility coefficients of phospholipid vesicles: experimental determination and theoretical modeling, J. Phys. Chem. 94 (1990) 4217–4223.
[71] W. Humphrey, A. Dalke, K. Schulten, VMD: visual molecular dynamics, J. Mol. Graph. 14 (1996) 33–38.
[72] E. Jurrus, D. Engel, K. Star, K. Monson, J. Brandi, L.E. Felberg, D.H. Brookes, L. Wilson, J. Chen, K. Liles, M. Chun, P. Li, D.W. Gohara, T. Dolinsky, R. Konecny, D.R. Koes, J.E. Nielsen, T. Head-Gordon, W. Geng, R. Krasny, G.W. Wei, M. J. Holst, J.A. McCammon, N.A. Baker, Improvements to the APBS biomolecular solvation software suite, Protein Sci. 27 (2018) 112–128.
[73] M. Pellegrini-Calace, T. Maiwald, J.M. Thornton, Pore-Walker: a novel tool for the identification and characterization of transmembrane protein channels from their three-dimensional structure, PLOS Comp. Biol. 5 (2009) 1–16.
[74] L. Pravda, D. Sehnal, D. Tousek, V. Navratilova, V. Bazgier, K. Berka, R. V. Svobodová, J. Koca, M. Otyepka, MOLEonline: a web-based tool for analyzing channels, tunnels and pores (2018 update), Nucleic Acids Res. 46 (2018) W368–W373.
[75] R.M. Cordeiro, Molecular dynamics simulations of the transport of reactive oxygen species by mammalian and plant aquaporins, Biochim. Biophys. Acta Gen. Subj. 1850 (2015) 1786–1794.
[76] W. Kabsch, A solution for the best rotation to relate two sets of vectors, Acta Crystallogr., Sect. A 32 (1976) 922–923.
[77] M.Y. Lobanov, N.S. Bogatyreva, O.V. Galzitskaya, Radius of gyration as an indicator of protein structure compactness, Mol. Biol. 42 (2008) 623–628.
[78] J.-C. Lin, H.-L. Liu, Protein conformational diseases: from mechanisms to drug designs, Curr. Drug Discov. Technol. 3 (2006) 145–153.
[79] A. Sannigrahi, N. De, K. Chattopadhyay, The bright and dark sides of protein conformational switches and the unifying forces of infections, Commun. Biol. 3 (2020) 382.
[80] C.O. Nwamba, K. Ibrahim, The role of protein conformational switches in pharmacology: its implications in metabolic reprogramming and protein evolution, Cell Biochem. Biophys. 68 (2014) 455–462.
[81] S.B. Ebrahimi, D. Samanta, Engineering protein-based therapeutics through structural and chemical design, Nat. Commun. 14 (2023) 2411.
[82] M.C. Oliveira, M. Yusupov, A. Bogaerts, R.M. Cordeiro, How do nitrated lipids affect the properties of phospholipid membranes? Arch. Biochem. Biophys. 695 (2020), 108548.
[83] M.C. Oliveira, M. Yusupov, A. Bogaerts, R.M. Cordeiro, Molecular dynamics simulations of mechanical stress on oxidized membranes, Biophys. Chem. 254 (2019), 106266.
[84] M.C. Oliveira, M. Yusupov, A. Bogaerts, R.M. Cordeiro, Lipid oxidation: role of membrane phase-separated domains, J. Chem. Inf. Model. 61 (2021) 2857–2868.
[85] J.F. Ek-Vitorin, J.M. Burt, Structural basis for the selective permeability of channels made of communicating junction proteins, Biochim. Biophys. Acta Biomembr. 1828 (2013) 51–68.
[86] S. Oh, T.A. Bargiello, Voltage regulation of connexin channel conductance, Yonsei Med. J. 56 (2015) 1–15.
[87] J. Kronengold, M. Srinivas, V.K. Verselis, The N-terminal half of the connexin protein contains the core elements of the pore and voltage gates, J. Membr. Biol. 245 (2012) 453–463.
[88] R. Jaradat, X. Li, H. Chen, P.B. Stathopulos, D. Bai, The hydrophobic residues in amino terminal domains of Cx46 and Cx50 are important for their gap junction ion permeation and gating, Int. J. Mol. Sci. 23 (2022), 11605.
[89] F. Zonta, D. Buratto, C. Cassini, M. Bortolozzi, F. Mammano, Molecular dynamics simulations highlight structural and functional alterations in deafness–related M34T mutation of connexin 26, Front. Physiol. 5 (2014) 85.
[90] S. Ramachandran, L.-H. Xie, S.A. John, S. Subramaniam, R. Lal, A novel role for connexin hemichannel in oxidative stress and smoking-induced cell injury, PLoS One 8 (2007), e712.
[91] R.-G. Xu, Z. Chen, M. Keidar, Y. Leng, The impact of radicals in cold atmospheric plasma on the structural modification of gap junction: a reactive molecular dynamics study, Int. J. Smart & Nano Mat. 10 (2019) 144–155.
[92] E. Cadenas, K.J. Davies, Mitochondrial free radical generation, oxidative stress, and aging, Free Radic. Biol. Med. 29 (2000) 222–230.
[93] I. Feine, I. Pinkas, Y. Salomon, A. Scherz, Local oxidative stress expansion through endothelial cells – a key role for gap junction intercellular communication, PLoS One 7 (2012), e41633.
[94] D.-P. Wu, L. Fan, C. Xu, Z. Liu, Y. Zhang, L. Liu, Q. Wang, L. Tao, GJIC Enhances the phototoxicity of photofrin-mediated photodynamic treatment by the mechanisms related with ROS and Calcium pathways, J. Biophot. 8 (2015) 765–774.
[95] S.N. Zucker, J. Zirnheld, A. Bagati, T.M. DiSanto, B. Des Soye, J.A. Wawrzyniak, K. Etemadi, M. Nikiforov, R. Berezney, Preferential induction of apoptotic cell death in melanoma cells as compared with normal keratinocytes using a non-thermal plasma torch, Cancer Biol. Ther. 13 (2012) 1299–1306.
[96] T.W. White, Functional analysis of human Cx26 mutations associated with deafness, Brain Res. Rev. 32 (2000) 181–183.
[97] B.C. Stong, Q. Chang, S. Ahmad, X. Lin, A novel mechanism for connexin 26 mutation linked deafness: cell death caused by leaky gap junction hemichannels, Laryngoscope 116 (2006) 2205–2210.
[98] L. Mei, J. Chen, L. Zong, Y. Zhu, C. Liang, R.O. Jones, H.-B. Zhao, A deafness mechanism of digenic Cx26 (GJB2) and Cx30 (GJB6) mutations: reduction of endocochlear potential by impairment of heterogeneous gap junctional function in the cochlear lateral wall, Neurobiol. Dis. 108 (2017) 195–203.
[99] A.D. Martínez, R. Acuña, V. Figueroa, J. Maripillan, B. Nicholson, Gap-junction channels dysfunction in deafness and hearing loss, Antioxidants Redox Signal. 11 (2009) 309–322.
[100] J. Kästner, *Umbrella sampling*, WIREs comput, Mol. Sci. 1 (2011) 932–942.
[101] M.C. Oliveira, H. Verswyvel, E. Smits, R.M. Cordeiro, A. Bogaerts, A. Lin, The pro- and anti-tumoral properties of gap junctions in cancer and their role in therapeutic strategies, Redox Biol. 57 (2022), 102503.